QSAR Analyses of the Substituted Indanone and Benzylpiperidine Rings of a Series of Indanone–Benzylpiperidine Inhibitors of Acetylcholinesterase

Mario G. Cardozo,[†] Youichi Iimura,[‡] Hachiro Sugimoto,[‡] Yoshiharu Yamanishi,[‡] and A. J. Hopfinger[*,†]

Department of Medicinal Chemistry and Pharmacognosy, M/C 781, University of Illinois at Chicago, P.O. Box 6998, Chicago, Illinois 60680 and Eisai Co., Ltd., Tsukuba Research Laboratories, 1-3, Tokodai 5 chome, Tsukuba, Ibaraki 300-26, Japan. Received June 19, 1991

QSAR analyses have been performed on the substituted indanone and benzylpiperidine ring substructures of a set of acetylcholinesterase, AChE, inhibitors of which 1-benzyl-4-[(5,6-dimethoxy-1-oxoindan-2-yl)methyl]piperidine hydrochloride is a potent in vitro and ex vivo inhibitor. The method of molecular decomposition–recomposition was used to define the sets of molecular substructures and corresponding in vitro inhibition databases. A QSAR involving the magnitude of the dipole moment, the highest occupied molecular orbital (HOMO) energy, and a specific π-orbital wave function coefficient of the substituted indanone ring substructure was constructed and found to be significant. The absence of any molecular-shape or bulk term in the QSAR, coupled with some of the relatively large substituents used to construct the QSAR, suggests considerable space is available around the indanone ring during the inhibition process. A set of QSARs were constructed and evaluated for substituents on the aromatic ring of the benzylpiperidine substructure. The most significant QSAR involves a representation of molecular shape, the largest principal moment of inertia, and the HOMO of the substituted aromatic ring. It appears that upon binding the receptor "wall" is closely fit around the benzyl ring, especially near the para position. Overall, the QSAR analysis suggests inhibition potency can be better enhanced by substitution on the indanone ring, as compared to the aromatic sites of the benzylpiperidine ring. Moreover, inhibition potency can be rapidly diminished, presumably through steric interactions with the receptor surface of AChE, by substitution of moderate to large groups on the benzyl ring, particularly at the para position.

Introduction

Reversible acetylcholinesterase (AChE) inhibitors have been tested as alternative drugs for Alzheimer's disease since the cholinergic function is selectively and irreversibly affected in this senile dementia disease.[1] In addition, transient memory enhancement with the AChE inhibitor physostigmine has been demonstrated in Alzheimer patients.[2] The mechanism proposed to explain the memory improvement is an increase of acetylcholine (ACh) levels in the central cholinergic synapses involved in the memory circuit by means of the inhibition of AChE. According to Giacobini,[3] drug-stimulated ACh hydrolysis inhibition, acting through a physiological mechanism, could maintain levels of ACh sufficient to stimulate postsynaptic receptors, and that such a mechanism could be more effective, and less toxic, than direct cholinergic stimulation by means of cholinomimetic agents. Different chemical classes of AChE inhibitors have been synthesized and evaluated as possible therapeutic agents in the treatment of Alzheimer's type of dementia.[4,5] A primary goal behind the synthesis of new series of AChE inhibitors has been to overcome the serious, and potentially lethal, side effects of short duration of action and a narrow therapeutic window of agents like physostigmine.

A novel new class of AChE inhibitors are the indanone–piperidine derivatives[6] of which 1-benzyl-4-[(5,6-dimethoxy-1-oxoindan-2-yl)methyl]piperidine hydrochloride (1) shows potent inhibitory action in both in vitro

(1)
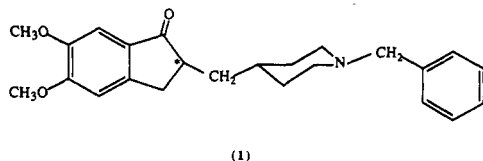
and ex vivo studies. The IC$_{50}$ of 1 in vitro is 5.3 nM as as compared to tetrahydroaminoacridine (52 nM) and physostigmine (0.43 nM).[7] Compound 1 inhibits AChE 570-
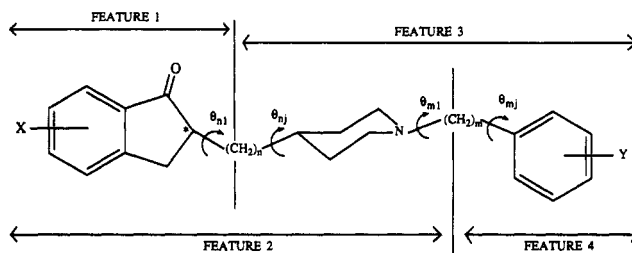

Figure 1. The four features of the indanone–benzylpiperidine AChE inhibitors defined.

fold more selectively than butyrylcholinesterease. In ex vivo experiments, 1 inhibited AChE in the brain of rat dose-dependently at 1–30 mg/kg, peritoneally.[8] This

(1) Drachman, D. A. Memory Dementia and Cholinergic System. In *Alzheimer's Disease: Senile Dementia and Related Disorders*; Katzman, R., Terry, R. D., Bick, K. L., Eds.; Raven Press: New York, 1978; pp 141–178.

(2) Perry, E. K.; Tomkinson, B. E.; Blessed, G.; Bergman, K.; Bigson, R. H.; Perry, R. H. Correlation of Cholinergic Abnormalities with Seniles Plaques and Mental Test Scores in Senile Dementia. *Br. Med. J.* **1978**, *2*, 1457–1459.

(3) Giacobini, E. Models and Strategies of Cholinergic Therapy of Alzheimer's Disease. In *Cholinergic Transmission in Pathophysiological Conditions*; Dowdall, M., Ed.; Ellis Horwood Ltd.: West Sussex, England, 1987; pp 882–901.

(4) Summers, W. K.; Visselman, J. O.; Marsh, G. M.; Tachiki, K.; Kling, A. Oral Tetrahydroaminoacridine in Long Term Treatment of Senile Dementia, Alzheimer Type. *New Eng. J. Med.* **1986**, *315*, 1241–1245.

(5) Marta, M.; Castellano, C.; Oliverio, A.; Pavone, F.; Pagella, P. G.; Brufani, M.; Pomponi, M. New Analogs of Physostigmine Alternative Drugs for Alzheimer's Disease? *Life Sci.* **1988**, *43*, 1921–1928.

(6) Iimura, Y.; Sugimoto, H.; Tsuchiya, Y.; Higurashi, K.; Karibe, N.; Sasaki, A.; Araki, S.; Yamanishi, Y.; Kawakami, Y.; Yamatsu, K. Structure-Activity Relationships of Acetylcholinesterase Inhibitors: Novel Piperidine Derivatives. 196th National Meeting of the American Chemical Society, Los Angeles, CA, Sept 25–30, 1988; MEDI-101.

(7) Araki, S.; Yamanishi, Y.; Kosasa, T.; Ogura, H.; Yamatsu, K. E2020, A Novel Centrally Acting Acetylcholinesterase Inhibitor (1): Inhibitory Action on Cholinesterase. *Proc. 62nd General Meeting Japanese Pharmacology Society*, 1989, Vol. 49, 0–299.

* Author to whom all correspondence should be sent.
† University of Illinois at Chicago.
‡ Eisai Co., Ltd.

inhibitory behavior of 1 is more potent, and longer lasting, than those of tetrahydroaminoacridine and physostigmine. Two other significant pharmacological features of 1 are antagonism of the decrease of ACh content in the frontal cortex induced by the lesion of nucleus basalis magnocellularis and the control of the depletion of ACh by scopolamine.[9] Analogues of 1 do not appear to act as direct, competitive inhibitors of ACh binding to AChE.

Given the therapeutic potential of the analogues of 1 we thought it worthwhile to perform both quantitative structure–activity relationship, QSAR, and molecular-modeling analyses on this class of AChE inhibitors. The goals of these studies are first to identify the physicochemical properties within the series that are responsible for AChE inhibition, and, secondly, to use this information to design new AChE inhibitors within this series, as well as to suggest novel leads. This paper reports the QSAR studies, and the following paper discusses the molecular-modeling analyses.

Methods

The molecular decomposition–recomposition, MDR, technique[10] has been used to carry out the combined QSAR and modeling studies of the indanone class of benzyl-piperidine inhibitors of AChE which are shown in Figure 1. This class of analogues was of primary focus in our studies. The MDR technique assumes that a molecule can be decomposed into a set of substructure molecules such that each set of individual substructure molecules can be analyzed, in terms of QSARs and/or molecular modeling, using the structure–activity data of the corresponding parent (whole) compounds. The selection of substructures is more art than science. The basic rule is to define the substructure such that the decomposed unit of interest is embedded in an environment that is analogous to that for the whole compound with respect to conformational and electronic properties.

Clearly, the MDR assumption is predicated upon selecting specific parent molecular structure–activity data in which the only changes in chemical structure occur in the substructure of interest. The remainder of the parent molecule remains constant for the substructure congeners being analyzed. MDR analysis also implicitly assumes that physicochemical changes in one substructure of the whole molecule do not modify the properties of any other substructure. That is, the substructures are uncoupled from one another with respect to the computation of molecular descriptors. Most often, conformational properties (spatial behavior) of the molecule must be explored in terms of substructure coupling. However, coupling of electronic properties should also be investigated in cases of resonance among/across selected substructures.

(8) Yamanishi, Y.; Araki, S.; Kosasa, T.; Ogura, H.; Yamatsu, K. Neurochemical Studies of E-2020, A Novel Centrally Acting Acetylcholinesterase Inhibitor. *Soc. Neurosci. Abstr.* **1988**, *27*, 20.

(9) Yamanishi, Y.; Kosasa, T.; Ogura, H.; Araki, S.; Yamatsu, K. E2020, A Novel Centrally Acting Acetylcholinesterase Inhibitor (2): Neurochemical Studies of Acetylcholine Metabolism. *Proc. 62nd General Meeting Japanese Pharmacology Society,* **1989**, Vol. 49, P-389.

(10) (a) Hopfinger, A. J.; Malhotra, D.; Battershell, R. D.; Ho, A.; Chen, J. A. Conformational Behavior and Thermodynamic Properties of Phenothrin Analog Insecticide. *Pest. Sci.* **1984**, *9*, 631–641. (b) Hopfinger, A. J.; Burke, B. J. Molecular Shape Analysis: A Formalism to Quantitatively Establish Spatial Molecular Similarity. In *Molecular Similarity;* Johnson, M. A., Maggiora, G. M., Eds.; John Wiley and Sons: New York, 1990; pp 173–209.

In this particular investigation the QSAR analyses are based upon molecular substructures that are bonded to the remainder of the parent compound by saturated single-carbon bonds. Thus, no resonance/electronic structure complications should occur in the estimation of electronic descriptors characteristic of a parent compound by using its substructure representative in a MDR–QSAR analysis. Also, the "length" and flexibility of the substituents used in the MDR–QSAR studies are sufficiently limited to alleviate any conformational coupling between a substructure and the remainder of the parent molecule. Hence, MDR–QSAR studies could be carried out for the indanone class of benzylpiperidine inhibitors of AChE with confidence that the MDR technique was applicable.

Conformation–activity relationships for the compound 1 class of AChE inhibitors were also explored within the framework of the MDR technique. However, it was necessary to "overlap" molecular substructures in order to take into account conformational coupling inherent to "adjacent" substructures. As is shown in the next paper, the overlap between substructures used to explore conformational profiles of the analogues of 1 using the MDR technique is achieved by having the piperidine ring common to the two substructures used to explore conformational behavior.

The benefit of using the MDR technique in exploring the conformation–activity relationship in a flexible analog series is to reduce the size of the conformational search. If the parent compound contains, say, N torsion angles that need to be searched, and it can be decomposed into M substructures each having T torsion angles, then an N dimensional search problem becomes M searches of dimension T. To put this in perspective, suppose $N = 10$ and $M = 5$ so that $T = 2$. Futher, let us assume that the search is carried out at 30° resolution (12 conformations are sampled per complete rotation) for each torsion angle. If the complete molecule is considered in the conformational search, 12^{10}, or about 62 billion conformations are explored. In contrast, the MDR technique requires that only 144 conformations need to be sampled on each of the five substructures!
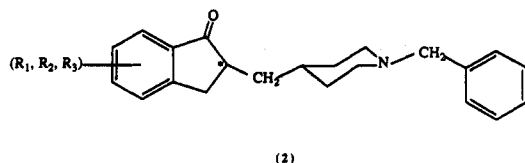
The inherent computational savings of using the MDR technique can also be realized when doing electronic property calculations. Rather than computing changes in the electronic structure of the entire parent compound due to a local substituent modification, it is more efficient to determine the changes in the electronic structure of the substructure containing the variable substituent. In essence, this reduces an N-electron structure calculation to one of less (often by a significant amount) than N electrons.

The indanone class of benzylpiperidine inhibitors of AChE was broken down into four structural components (features) with respect to the development of structure–activity models. The four features are defined in Figure 1. Feature 1 encompases substitutions on the indanone ring while feature 4 delineates substituent patterns in the benzyl ring joined to the piperidine ring.

This paper deals with the derivation of QSARs for features 1 and 4 using a combination of modeling, electronic-structure calculations, and linear free energy techniques to generate QSAR descriptors.

1. Feature 1. The set of 18 analogues reported in Table I were used to develop the feature 1 QSARs. These compounds were selected because all of them have the same general structure, **2**, so that the only way the structures differ from one another is in the substituents (R_1, R_2, R_3) on the aromatic ring of the indanone bicycle. Thus, the

(2)

SAR for this set of compounds is due only to (R_1, R_2, R_3), and the MDR technique can be applied. In general, isomers at the *-carbon of the indanone ring are not resolved with respect to inhibition potency. The following paper[11] does incorporate the role of this chiral center on molecular conformation. The spacer link from C* to the piperidine ring is at least partially saturated, and in most cases totally saturated, so that resonance effects from substituent modifications on the rest of the molecule can be neglected.

The range in AChE inhibition potency for the 18 analogues is 1.3–380 nM IC_{50} units, where IC_{50} indicates the concentration of analogue necessary for 50% inhibition of AChE.

Conformational and electronic descriptors were determined using the model compound **3** to represent all analogues **2**.

(3)
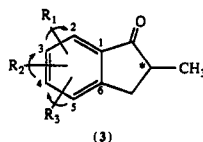
The valence geometry of the unsubstituted model compound **3** was built from chemical fragments available on the CHEMLAB-II library.[12] This structure was fully optimized using the MNDO[13] method for $R_1 = R_2 = R_3 = H$ and held fixed in all subsequent feature 1 calculations. The (R_1, R_2, R_3) analogues of **3** were constructed from appropriate chemical fragments using the same library as described above. Minimum intramolecular energy conformer states of all flexible substituents of Table I, except for compounds **5, 10, 13, 16**, and **17**, were generated by scanning about appropriate torsion angles and computing the fixed valence geometry molecular mechanics energy.[14] The methyl group of the substituent on the aromatic ring was treated as unified atomic group.[15] In addition, the torsion angles about the oxygen–alkyl carbon atom for compounds **3** and **6** were also scanned. Torsion angle scans were carried out at 30 increments, and the MM2 nonbonded potentials[16] were used in combination with a Coulombic electrostatic potential (employing MNDO Coulson partial charges) to estimate the conformational energy. Intrinsic torsion potential functions were included when necessary.[14] Local minimum energy conformer states up to 5 kcal/mol above the apparent global minimum were used as starting points for subsequent fixed-valence ge-

ometry energy minimizations. Each stable intramolecular conformer for a flexible substituent was used to compute the magnitudes of QSAR descriptors that are dependent upon conformation, for example, dipole moment. Table II summarizes the set of minimum intramolecular energy conformations considered in the construction of the QSAR equation. Each such measure was considered in constructing trial QSARs. The following set of descriptors was used in the QSAR analysis of feature 1: (1) Partial charge densities (from MNDO) on the C_1 to C_6 carbon atoms in **3**. (2) Total dipole moment, U_T, and the angle the dipole makes with the C=O bond in the plane of the indanone ring. (3) Component of the dipole moment in the C=O direction, U_Z. (4) Lowest unoccupied molecular orbital energy, LUMO. (5) Highest occupied molecular orbital energy, HOMO. (6) Atomic orbital electron populations in C_3, C_4, and C_5. (7) Sum of the atomic orbital electron populations in C_1 through C_6. (8) Sum of the atomic orbital electron populations in C_1 through C_6 plus C_9 and O_{10}. (9) HOMO π coefficient of each of the phenyl carbons C_1 through C_6 as well as O_{10}. (10) Sum of the squares of the HOMO π coefficients of C_1 through C_6 plus C_9 and O_{10}. (11) Partition coefficient, log P,[17] of **3**.

2. Feature 4. The set of 16 analogues given in Table III were used to develop feature 4 QSARs. These compounds were selected because all of them have the same general structure. The only way in which these compounds differ from one another is in the substituent Y. Thus, model compound **4** was used as the substructure in applying the MDR technique for the feature 4 QSAR analysis.

(4)
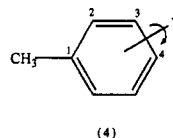
The range in AChE IC_{50}'s for the 16 analogues is 1–4900 nM. This is a reasonably large range in inhibition potency from the point of view of constructing statistically significant correlation relationships. For Y substituents having conformational flexibility, the same molecular-modeling and conformational analysis procedures described for (R_1, R_2, R_3) of feature 1 were used to determine the minimum energy conformer states of Y. Once again, each intramolecular minimum energy conformer state was used to compute measures of descriptors that are dependent upon substituent conformation. Each descriptor measure was considered in the QSAR analysis.

The following set of descriptors were used as part of the feature 4 QSAR study: (1) The nonoverlap steric volume, S_0, using the aromatic ring as the molecular superposition criterium. (2) The principal moments of inertia of **4**. (3) The center of charge of **4** relative to the 1-methyl carbon. (4) The highest occupied molecular orbital (HOMO) energy. (5) The partition coefficient, log P, of **4**.

Trial QSARs were generated by considering all combinations of the descriptors for both feature 1 and feature 4. Both linear and quadratic descriptor terms were used in the set of multidimensional linear regression analyses. The SAS package[18] was used to do the statistical analyses.
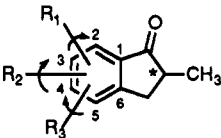
Results

The optimum QSAR that could be constructed for

(11) Cardozo, M. G.; Hopfinger, A. J. Conformational and Molecular Shape Analyses of Some Benzyl Piperidine AChE Inhibitors, following paper.

(12) CHEMLAB-II V11.0. Distributed by Polygen-Molecular Simulations, 200 Fifth Ave., Waltham, MA 02254; 1991.

(13) Dewar, M. J. S.; Thiel, W. Ground States of Molecules. 38. The MNDO Method Approximation and Parameters. *J. Am. Chem. Soc.* **1977**, *99*, 4899–4907.

(14) Hopfinger, A. J. *Conformational Properties of Macromolecules*; Academic Press: New York, 1973; pp 38–131.

(15) Mabilia, M.; Pearlstein, R. A.; Hopfinger, A. J. Molecular Shape Analysis and Energetics-Based Intermolecular Modelling of Benzylpyrimidine Dihydrofolate Reductase Inhibitors. *Eur. J. Med. Chem.* **1985**, *20*, 163–174.

(16) Allinger, N. L. Conformational Analyses. 130. MM2. A Hydrocarbon Force Field Utilizing V1 and V2 Torsional Terms. *J. Am. Chem. Soc.* **1977**, *99*, 8127–8134.

(17) MedChem Software V3.54. Daylight Chemical Information Systems, Inc.: Irvine, CA 92715; 1989.

(18) Draper, N. R.; Smith, H. *Applied Regression Analyses*; Wiley and Sons: New York, 1966.

Table I. General SAR Data for Feature 1, Based on the Model Compound 3

no.	R_1	R_2	R_3	C_4	U_T Debye	HOMO energy (eV)	obs $-\log(IC_{50})$	cal (eq 1) $-\log(IC_{50})$	obs $-$ cal (eq 1) $-\log(IC_{50})$	cal (eq 2) $-\log(IC_{50})$	obs $-$ cal (eq 2) $-\log(IC_{50})$
1	3-OH	4-OMe	H	0.356	3.918	-9.305	8.88	8.46	0.42	8.81	0.07
2	3-OMe	4-OMe	H	0.454	2.301	-9.533	8.28	7.38	0.90	8.20	0.08
3	3-OEt	4-OEt	H	0.505	2.855	-9.631	8.20	8.00	0.20	7.86	0.34
5	H	H	5-Me	0.234	2.966	-9.593	8.15	7.46	0.69		
6	3-OMe	4-O-isop	H	0.449	3.332	-9.451	8.05	8.48	-0.43	8.19	-0.14
7	H	H	5-OMe	0.249	3.127	-9.545	7.92	7.72	0.20	7.55	0.37
8	2-OMe	3-OMe	4-OMe	0.468	2.765	-9.615	7.88	7.84	0.04	7.82	0.06
9	H	4-OMe	5-OMe	0.452	2.629	-9.461	7.70	7.77	-0.07	7.93	-0.23
10	3,4-methylenedioxy	H		0.409	2.785	-9.314	7.64	7.58	0.06	7.51	0.13
11	2-OMe	4-OMe	H	0.364	2.845	-9.581	7.60	7.70	-0.10	7.64	-0.04
12	2-OMe	H	5-OMe	0.251	3.248	-9.443	7.44	7.86	-0.42	7.65	-0.21
13	3-Me	H	H	0.168	3.004	-0.615	7.16	7.27	-0.11	7.19	-0.03
14	3-OMe	H	H	0.247	2.980	-9.577	7.09	7.53	-0.44	7.42	-0.33
15	2-OMe	3-OMe	H	0.027	3.192	-9.376	7.06	7.10	-0.04	7.00	0.06
16	H	H	H	0.021	3.009	-9.716	6.83	6.58	0.25	6.58	0.25
17	3-F	H	H	0.226	3.467	-9.856	6.70	6.90	-0.20	6.80	-0.10
18	3-OMe	4-OH	H	0.463	1.946	-9.508	6.42	6.97	-0.55		

Table II. Summary of Torsion Angles for Substituents of the Model Compound 3

compd	torsion angles[a] θ_1	θ_2	θ_3	$\theta_{1'}$	$\theta_{2'}$	E^b	compd	torsion angles[a] θ_1	θ_2	θ_3	$\theta_{1'}$	$\theta_{2'}$	E^b
1-M1	177[c]	84[d]				0.0	M2	91	-88	93			0.2
M2	175	-82				0.1	9-M1		112[d]	-104[i]			0.0
M3	72	75				0.3	M2		-102	106			0.1
M4	71	-74				0.4	M3		-91	-113			0.8
M5	177	178				0.4	M4		3	-118			2.3
2-M1	78[e]	-73[d]				0.0	11-M1	91[j]	-89[e]				0.0
M2	-81	74				0.0	M2	90	89				0.0
M3	67	83				0.1	M3	-89	-88				0.0
M4	-68	-85				0.2	M4	-90	91				0.0
M5	28	179				2.4	12-M1	93[j]		-73[i]			0.0
3-M1	-119[e]	-88[d]		180[f]	180[g]	0.0	M2	81		76			0.1
M2	89	-91		180	180	0.1	M3	88		-68			0.3
M3	90	-61		180	180	0.4	M4	-89		71			0.4
M4	-89	-119		180	180	0.5	14-M1	84[e]	3[k]				0.0
4-M1		76[d]				0.0	M2	76	-53				0.2
M2		-80				0.2	M3	-76	53				0.2
M3		2				1.8	M4	74	54				0.3
M4		179				1.9	M5	-70	-50				0.3
6-M1	-92[e]	-59[d]			-61[h]	0.0	15-M1	-118[j]	-91[e]				0.0
M2	90	-89			90	0.3	M2	-119	92				0.1
M3	62	-61			-59	1.0	M3	119	122				0.4
M4	91	-118			62	1.0	M4	-91	-118				0.6
M5	-90	89			-91	1.5	M5	89	179				2.5
7-M1			74[i]			0.0	18-M1	-75[e]					0.0
M2			-70			0.4	M2	82					0.1
M3			-2			2.2	M3	179					1.8
8-M1	-92[j]	89[e]	-61[d]			0.0	M4	1					1.9

[a] The torsion angle θ_n of the bonded atoms abcd adopt the value of 0° for the cis-planar arrangement of the bond ab and bc. [b] Difference in conformational energy respect to the global minimum in kilocalories per mole. [c] For this compound θ_1 is the torsion angle between the bonds C_2-C_3 of the aromatic ring and O-H of the substituent at position 3. [d] For this compound θ_2 is the torsion angle between the bonds C_3-C_4 of the aromatic ring and O-CH_3 of the substituent at position 4. [e] For this compound θ_1 is the torsion angle between the bonds C_2-C_3 of the aromatic ring and O-CH_3 of the substituent at position 3. [f] For this compound $\theta_{1'}$ is the torsion angle between the atoms C_3-O-C-H_2-CH_3 of the substituent at position 3. [g] For this compound $\theta_{2'}$ is the torsion angle between the atoms C_4-O-CH_2-CH_3 of the substituent at position 4. [h] For this compound $\theta_{2'}$ is the torsion angle between the atoms C_4-O-CH-CH_3b of the substituent at position 4. [i] For this compound θ_3 is the torsion angle between the bonds C_4-C_5 of the aromatic ring and O-CH_3 of the substituent at position 5. [j] For this compound θ_1 is the torsion angle between the bonds C_1-C_2 of the aromatic ring and O-CH_3 of the substituent at position 2. [k] For this compound θ_2 is the torsion angle between the bonds C_2-C_3 of the aromatic ring and O-H of the substituent at position 4.

substitution onto the aromatic unit of the indanone ring, based upon all of the analogues in Table I, is

$$-\log (IC_{50}) = 2.73[C_4] + 1.86[U_T] - 0.14[U_T^2] - 156.7[HOMO] - 8.25[HOMO^2] - 740.93 \quad (1)$$

$N = 18; R = 0.804; SD = 0.46; F = 4.4; U_T(max) = 6.6debye; HOMO(max) = -9.49 eV$

where C_4 is the HOMO out-of-plane π orbital coefficient of ring carbon four, and the other terms in eq 1 have already been explicitly defined. An analysis of the residual of fit, $\Delta \log (IC_{50}) = (-\log (IC_{50}))_{obs} - (-\log (IC_{50}))_{cal}$, of eq 1 indicates that the marginal fit of this correlation equation is largely due to two outliers—compounds 5 and 18 of Table I. Compound 5 is predicted to be less active than

Table III. General SAR Data for Feature 4, Based on the Model Compound 4
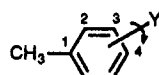
no.	Y	S_0 (Å^3)	IX	HOMO energy (eV)	obs $-\log$ (IC_{50})	cal $-\log$ (IC_{50})	obs $-$ cal $-\log$ (IC_{50})
1	3-F	0.86	17.47	-9.549	9.00	8.93	0.07
2	4-OH	6.80	15.24	-8.910	8.74	8.08	0.66
3	3-Me	11.47	23.46	-9.286	8.70	8.02	0.68
4	3-NO$_2$	14.06	31.96	-10.342	8.40	8.31	0.09
5	H	0.71	15.72	-9.339	8.28	8.83	-0.55
6	2-F	6.94	26.19	-9.527	8.02	8.67	-0.65
7	4-F	3.69	15.23	-9.478	8.02	8.51	-0.49
8	2-Me	21.40	26.57	-9.262	8.00	7.10	0.90
9	4-NH$_2$	9.72	15.47	-8.117	7.44	7.65	-0.21
10	4-Me	17.33	15.72	-9.225	7.40	7.03	0.37
11	3-OH				7.34		
12	4-NO$_2$	19.20	22.31	-10.391	7.00	7.32	-0.32
13	3-OMe	18.83	23.55	-8.954	6.66	7.19	-0.53
14	4-OMe	25.37	17.47	-8.895	5.44	6.20	-0.76
15	3,4-OMe	48.19	62.97	-9.198	5.40	5.90	-0.50
16	3,4,5-OMe	70.83	102.57	-9.367	5.31	5.32	-0.01

observed, while the opposite is true for 18.

If compounds 5 and 18 are not considered in the analysis, then the structure–activity data set of the remaining 16 compounds can be described by a significant QSAR,

$$-\log (IC_{50}) = 2.21[C_4] - 6.65[U_T] + 1.18[U^2_T] - 162.9[HOMO] - 8.58[HOMO^2] - 757.52 \quad (2)$$

$$N = 16; R = 0.939; SD = 0.25; F = 14.8; U_T(\text{max}) = 2.8 \text{ debye}; HOMO(\text{max}) = -9.49 \text{ eV}$$

At first inspection the most obvious difference between eqs 1 and 2, besides the considerable increase in statistical significance of eq 2, is the change in the dependence of $-\log$ (IC_{50}) on U_T. According to eq 2, $-\log$ (IC_{50}) increases with increasing U_T for $U_T > 2.8$ debye, while for eq 1, $-\log$ (IC_{50}) decreases as U_T increases for $U_T > 6.6$ debye. However, these two relationships between $-\log$ (IC_{50}) and U_T are not inconsistent for most of the analogues in Table I. Fifteen of the eighteen compounds in Table I have U_T values in the 2.8–6.6 debye range. Both eqs 1 and 2 predict $-\log$ (IC_{50}) to increase with increasing U_T in this range of dipole values. The dependence of $-\log$ (IC_{50}) on HOMO is virtually identical in eqs 1 and 2.

For feature 4 the optimum QSAR that could be developed is

$$-\log (IC_{50}) = -0.107[S_0] + 0.046[IX] - 0.151[HOMO] + 6.683 \quad (3)$$

$$N = 15; R = 0.905; SD = 0.60; F = 16.7$$

In eq 3 S_0 is the nonoverlap steric volume between each analogue and the shape reference compound (Y = 3-OH) and IX is the largest principal moment of inertia of each analogue as represented by 4. The shape reference compound was determined by seeing which of the 16 analogues, each tested as the shape reference, gave the statistically most significant QSAR. Compound 8 (Y = 2-Me), of Table III is the largest outlier for the QSAR given by eq 3. The values of the QSAR descriptors, the predicted $-\log$ (IC_{50})'s, and the corresponding residuals of fit are reported as part of Table III.

Discussion

The decomposition of the indanone–benzylpiperidines into four structural components (features), for purposes of QSAR and molecular-modeling analyses, imposes a major constraint. This constraint requires that for the structure–activity exploration of any one feature, the other

Table IV. Para Substituents, Y, of Feature 4, Their Steric Lengths (Sizes), and Observed $-\log$ (IC_{50})s

Y	steric length (Å)	$-\log$ (IC_{50})
H	2.23	8.28
F	2.60	8.02
OH	3.15	8.74
NH$_2$	3.20	7.44
CH$_3$	3.36	7.40
NO$_2$	3.92	7.00
OCH$_3$	4.84	5.44

three features must be held fixed. Consequently, the size of a data set for any single feature is normally less than the actual number of analogues synthesized and tested when using the MDR technique.

AChE inhibition appears to be less sensitive, with respect to major losses in potency, for substitutions onto the indanone ring (R_1, R_2, R_3), as compared to substitutions on the aromatic ring Y. This observation, coupled with the presence of a steric shape term in eq 3, suggests that substructure 4 is in a more restricted steric environment than 3 when ligand–receptor binding occurs for the indanone–benzylpiperidines with AChE. Moreover, loss in inhibition potency seems particularly sensitive to the size of the Y substituent in the para position. This trend can be seen in Table IV where the type and size (steric length) of para substituents are reported along with the corresponding $-\log$ (IC_{50}). Using the unsubstituted ring as a reference, AChE inhibition potency decreases with increasing steric length of the para Y substituent. The only exception to this relationship is Y = 4-OH which is also predicted to less active by eq 3 than is observed (see Table III).

The magnitude of the dipole, U_T, of the substituted indanone ring is the most significant descriptor in eq 2. The parabolic dependence of $-\log$ (IC_{50}) on U_T may be an artifact of the regression fit. Most dipoles in Table I have a magnitude greater than 2.8, the value which corresponds to minimizing $-\log$ (IC_{50}) as a function of U_T. Thus, most of the analogues used to construct eq 2 can be reasonably treated by a QSAR that expresses a linear relationship between $-\log$ (IC_{50}) and U_T.

One test of the QSAR given by eq 2 was the synthesis and testing of [R_1 = 2-CN, R_2 = 5-OCH$_3$, R_3 = H] which should have been quite active according to the QSAR. It was not active. A comparison of [R_1 = 2-OCH$_3$, R_2 = 3-OCH$_3$, R_3 = 4-OCH$_3$], see Figure 2, which is a quite active
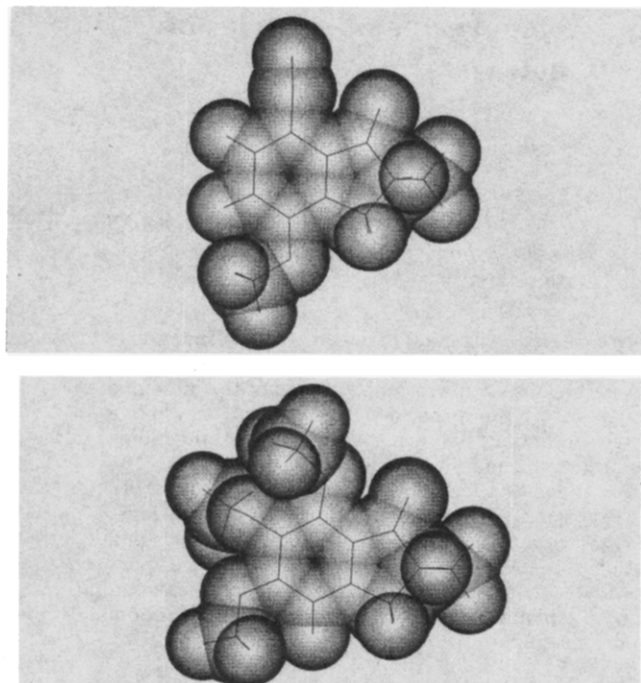
Figure 2. A spatial comparison of the inactive analogue (A, top) [R_1 = 2-CN, R_2 = 5-OCH$_3$, R_3 = H] to the active AChE inhibitor (B, bottom) [R_1 = 2-OCH$_3$, R_2 = 3-OCH$_3$, R_3 = 4-OCH$_3$]. Note the length of the 2-CN in the plane of the indanone ring.

analogue, suggests that the length of the 2-CN substituent, in the direction of C—CN bond, may block intermolecular hydrogen bonding with a receptor site involving the C=O of the indanone ring. Rotation about the C(ring)—C≡N bond does not alter the location of cyano nitrogen in space. However, the C(ring)—OCH$_3$ rotation can place the methyl group in different spatial locations, out of the "plane" of the indanone ring to which the cyano nitrogen is restricted. Also, the negative charge of the nitrogen could confuse a proton donor trying to hydrogen bond to the oxygen of the indanone ring. While this explanation of the inactivity of the [R_1 = 2-CN, R_2 = 5-OCH$_3$, R_3 = H] is tentative, we also note that the absence of the C=O in a 6–5 bicycle ring

analogue to 1 is also inactive. Further, the lengths of p-CN and p-phenyl groups could be used to quantitatively explain the inactivity of the corresponding analogues in a previous QSAR study.[19]

It is tempting to be critical of an incorrect prediction of activity like that made for the [R_1 = 2-CN, R_2 = 5-OCH$_3$, R_3 = H] analogue. However, it may be better to view such a "failure" as mapping out additional structural requirements for activity that cannot be gleaned from the information inherent to an existing structure–activity data set.

Registry No. 1, 120014-06-4; **3** (R_1 = 3-OH, R_2 = 4-OMe, R_3 = H), 138261-07-1; **3** (R_1 = 3-OMe, R_2 = 4-OMe, R_3 = H), 4191-17-7; **3** (R_1 = 3-OEt, R_2 = 4-OEt, R_3 = H), 138261-08-2; **3** (R_1 = H, R_1 = 4-OMe, R_3 = H), 60848-62-6; **3** (R_1 = R_2 = H, R_3 = 5-Me), 64919-47-7; **3** (R_1 = 3-OMe, R_2 = 4-Oisop, R_3 = H), 138261-09-3; **3** (R_1 = R_2 = H, R_3 = 5-OMe), 105372-23-4; **3** (R_1 = 2-OMe, R_2 = 3-OMe, R_3 = 4-OMe), 4087-69-8; **3** (R_1 = H, R_2 = 4-OMe, R_3 = 5-OMe), 138261-10-6; **3** (R_1 = R_2 = 3,4-methylenedioxy, R_3 = H), 51003-79-3; **3** (R_1 = 2-OMe, R_2 = 4-OMe, R_3 = H), 61227-52-9; **3** (R_1 = 2-OMe, R_2 = H, R_3 = 5-OMe), 59743-69-0; **3** (R_1 = 3-Me, R_2 = R_3 = H), 66309-83-9; **3** (R_1 = 3-OMe, R_2 = R_3 = H), 5464-10-8; **3** (R_1 = 2-OMe, R_2 = 3-OMe, R_3 = H), 138261-11-7; **3** (R_1 = R_2 = R_3 = H), 17496-14-9; **3** (R_1 = 3-F, R_2 = R_3 = H), 37794-19-7; **3** (R_1 = 3-OMe, R_2 = 4-OH, R_3 = H), 137542-56-4; **4** (Y = 3-F), 352-70-5; **4** (Y = 4-OH), 106-44-5; **4** (Y = 3-Me), 108-38-3; **4** (Y = 3-NO$_2$), 99-08-1; **4** (Y = H), 62-53-3; **4** (Y = 2-F), 95-52-3; **4** (Y = 4-F), 352-32-9; **4** (Y = 2-Me), 95-47-6; **4** (Y = 4-NH$_2$), 106-49-0; **4** (Y = 4-Me), 106-42-3; **4** (Y = 3-OH), 108-39-4; **4** (Y = 4-NO$_2$), 99-99-0; **4** (Y = 3-OMe), 100-84-5; **4** (Y = 4-OMe), 104-93-8; **4** (Y = 3,4-OMe), 494-99-5; **4** (Y = 3,4,5-OMe), 6443-69-2; AChE, 9000-81-1.

(19) Hopfinger, A. J. A QSAR Investigation of Dihydrofolate Reductase Inhibition by Baker Triazines Based Upon Molecular Shape Analysis. *J. Am. Chem. Soc.* **1980**, *102*, 7196–7206.